Catalysis and Structural Properties of *Leishmania infantum* Glyoxalase II: Trypanothione Specificity and Phylogeny[†,‡]

Marta Sousa Silva,[§,||,⊥] Lídia Barata,[§,⊥] António E. N. Ferreira,[§] Susana Romão,[||] Ana M. Tomás,[||,▽] Ana Ponces Freire,[§] and Carlos Cordeiro*[,§]

Centro de Química e Bioquímica, Departamento de Química e Bioquímica, Faculdade de Ciências da Universidade de Lisboa, Lisboa, and Institutos de Biologia Molecular e Celular (IBMC) and de Ciências Biomédicas Abel Salazar (ICBAS), Universidade do Porto, Porto, Portugal

Received May 22, 2007; Revised Manuscript Received October 18, 2007

ABSTRACT: The glyoxalase pathway catalyzes the formation of D-lactate from methylglyoxal, a toxic byproduct of glycolysis. In trypanosomatids, trypanothione replaces glutathione in this pathway, making it a potential drug target, since its selective inhibition might increase methylglyoxal concentration in the parasites. Two glyoxalase II structures were solved. One with a bound spermidine molecule (1.8 Å) and the other with D-lactate at the active site (1.9 Å). The second structure was obtained by crystal soaking with the enzyme substrate (*S*)-D-lactoyltrypanothione. The overall structure of *Leishmania infantum* glyoxalase II is very similar to its human counterpart, with important differences at the substrate binding site. The crystal structure of *L. infantum* glyoxalase II is the first structure of this enzyme from trypanosomatids. The differential specificity of glyoxalase II toward glutathione and trypanothione moieties was revealed by differential substrate binding. Evolutionary analysis shows that trypanosomatid glyoxalases II diverged early from eukaryotic enzymes, being unrelated to prokaryotic proteins.

The trypanosomatids are the etiological agents of several human and animal diseases, widespread in the third world and in the Mediterranean basin. Emergent target populations for leishmaniasis are HIV patients and people following immunosupressor therapies. No curative drugs or vaccines currently exist, and actual therapeutic approaches are becoming limited given their undesirable side effects and the evolution of resistant forms of trypanosomatids. Novel and effective therapeutic approaches are much needed, and these must rely on unique physiological and biochemical properties of trypanosomatids. These intracellular eukaryotic parasites have a complex life cycle, requiring an insect vector for transmission to a mammalian host. Unique cytological features are the presence of a single large mitochondrion containing the kinetoplast DNA and a singular compartment, the glycosome, where the major part of glycolysis takes place (*1*, *2*). However, the most remarkable biochemical characteristic of trypanosomatids is the functional replacement of glutathione by trypanothione (N^1,N^8-bis(glutathionyl)spermidine), a spermidine−glutathione conjugate (*3*, *4*). This thiol fulfills the role of glutathione in the detoxification of metals, drugs, hydroperoxides, peroxynitrite, and ketoaldehydes (*5*). Glutathione-dependent enzymes in trypanosomatids are replaced by functionally analogous enzymes that specifically use trypanothione. For instance, trypanothione reductase replaces glutathione reductase, while thioredoxin-dependent processes are replaced by the tryparedoxin system (*4*). Not surprisingly, trypanothione is essential, and therefore, targeting its biosynthesis or trypanothione-dependent enzymes with inhibitors will provide a synergistic effect with deleterious consequences to the parasite, while leaving unaffected the host glutathione-dependent processes. To achieve this goal, the focus should be placed on researching the molecular basis of trypanothione specificity. An ideal model is glyoxalase II, an enzyme from the glyoxalase system. Through the sequential action of glyoxalase I (lactoylglutathione lyase, EC 4.4.1.5) and glyoxalase II ((hydroxyacyl)glutathione hydrolase, EC 3.1.2.6), D-lactate is produced from methylglyoxal using glutathione in every living cell (*6*), except in trypanosomatids where the thiol is trypanothione (*7*−*9*). Glyoxalase I catalyzes the formation of lactoyltrypanothione from the hemithioacetal formed nonenzymatically from methylglyoxal and trypanothione, while glyoxalase II hydrolyzes this thioester, forming D-lactate and regenerating trypanothione. Both enzymes catalyze virtually irreversible reactions, and glyoxalase II shows absolute specificity toward the trypanothione moiety in lactoyltrypanothione (*8*, *9*).

In the present study, recombinant *Leishmania infantum* glyoxalase II (*Li*GLO2)[1] was purified and kinetically characterized. Its crystal structure was solved by molecular replacement, using the crystal structure of the glutathione-

[†] Supported by Projects POCTI/ESP/48272/2002 and POCI/QUI/62027/2004 and by Grants SFRH/BPD/28345/2006 (to M.S.S.) and SFRH/BD/28691/2006 (to L.B.) from the Fundação para a Ciência e a Tecnologia, Ministério da Ciência e Tecnologia, Portugal.

[‡] The *LiGLO2* sequence was deposited in GenBank (accession no. DQ294972). The glyoxalase II three-dimensional structures *Li*GLO2−spermidine and *Li*GLO2−D-lactate were deposited in the Protein Data Bank (PDB ID codes 2P18 and 2P1E).

* To whom correspondence should be addressed. Fax: 351-217500088. Phone: +351.217500929. E-mail: cacordeiro@fc.ul.pt.

[§] Faculdade de Ciências da Universidade de Lisboa.

[||] IBMC, Universidade do Porto.

[⊥] These authors contributed equally to this work.

[▽] ICBAS, Universidade do Porto.

10.1021/bi700989m CCC: $40.75
Published on Web 12/06/2007

dependent human glyoxalase II (*10*). Several highly conserved residues are shared by the trypanosomatid and human glyoxalases II at the active site. This is not surprising since the catalyzed reaction is chemically identical and both are metallo-β-lactamases containing zinc or iron at the active site. However, some residues are unique to the trypanosomatid enzyme, and their location close to the active site explains the differential substrate specificity. This is the first report of the glyoxalase II structure from a trypanosomatid. The presence of an extra density compatible with a spermidine molecule bound close to the active site allowed us to understand why trypanosomatid glyoxalases II are specific toward trypanothione substrates.

EXPERIMENTAL PROCEDURES

Protein Expression and Purification. The *LiGLO2* gene was amplified from *L. infantum* (clone MHOM/MA67ITMAP263) genomic DNA by PCR with specific primers, as previously reported (*11*). Briefly, the sense primer (5′-ccgcgcacatatgcgcaactactgcac-3′) contained the *Nde*I site (underlined) and the start ATG (italic); the antisense primer (5′-caccgctcgagtcagtcgcaggcgttgt-3′) contained the *Xho*I site (underlined) immediately after the stop codon. The gene was amplified from genomic DNA using the PWO polymerase (GibcoBRL, Paisley, Scotland), as follows: 94 °C for 2 min, 48 °C for 1 min, 72 °C for 1 min (2 cycles); 94 °C for 45 s, 62 °C for 1 min, 72 °C for 1 min (30 cycles); 72 °C for 10 min. The gene was cloned into the prokaryotic expression vector pET-28a (Novagen, Madison, WI), using the referred restriction sites, and *Escherichia coli* BL21-codon plus (Stratagene) was transformed with the pET-28a/his-*LiGLO2* plasmid. Sequencing of the open reading frame was carried out prior to protein expression.

For overexpression of His_6-*Li*GLO2 (a fusion protein, with an N-terminal tail of six histidines and a thrombin cleavage site; the total tag sequence including linker and cleavage site is MGSSHHHHHHSSGLVPRGSH), transformants were grown in 3 L of LB medium containing 50 $\mu g \cdot mL^{-1}$ kanamycin and 100 $\mu g \cdot mL^{-1}$ chloramphenicol, at 37 °C. When the culture reached an $OD_{600\ nm}$ of 0.6, expression was induced with 0.2 mM isopropyl β-D-thiogalactopyranoside (IPTG) for 3 h at 37 °C. After induction, the bacteria were pelleted, resuspended in 120 mL of 500 mM NaCl, 20 mM Tris−HCl, pH 7.6, and lysed by sonication, and the cell debris was removed by centrifugation at 10000*g* for 30 min at 4 °C. The fusion protein was purified at 4 °C by chromatography on a His Bind resin (Novagen) column (XK 26/20, Amersham Pharmacia Biotech, Uppsala, Sweden). His-*Li*GLO2 was eluted with an imidazole gradient from 5 mM to 1 M at a flow rate of 2.5 $mL \cdot min^{-1}$. Fractions confirmed to contain *Li*GLO2 by SDS−PAGE were pooled, applied to PD-10 columns (Amersham Biosciences), and eluted with 1× PBS, pH 7.4. The purity of the recombinant *L. infantum* His-*Li*GLO2 was ≥95%, as estimated by SDS−PAGE and gel filtration chromatography. His-*Li*GLO2 was concentrated using Amicon Ultra-4 filters (10 000 NMWL, Millipore Corp., Molsheim, France) and further purified by FPLC with an LKB 2050 pump (LKB-Bromma) using a Superdex 75 10/300 GL column (Amersham Biosciences) and a Jasco UV-2075 Plus detector at 280 nm with a flow of 0.4 $mL \cdot min^{-1}$ in 150 mM NaCl and 20 mM KH_2PO_4. The protein concentration was determined using the Bio-Rad protein assay dye reagent (Bio-Rad, Hercules, CA).

Crystallization. Crystals were grown within 2 days, at 288 K, in hanging drops, as described previously (*11*), containing 2 μL of well liquor consisting of 30% (w/v) PEG 8000, 0.2 M $MgCl_2$, and 0.1 M acetate, pH 5.5, mixed with 1 μL of 25 $mg \cdot mL^{-1}$ recombinant glyoxalase II in 10 mM Hepes, pH 7.0. All data were collected from crystals frozen in liquid nitrogen.

Crystal Structure Determination. A high-resolution complete native data set was collected at 100 K at beamline ID14-1 as described previously (*11*) and at beamline ID23-1 at the European Synchrotron Radiation Facility (ESRF) in Grenoble, France. Data were processed using MOSFLM (*12*) and scaled using SCALA from the CCP4 program package (*13*). The structures were solved by molecular replacement using the structure of the human homologue as a search model and the program Phaser (*14*) from the CCP4 suite. Manual model building was performed using COOT (*15*). Refmac5 from the CCP4 suite and all data were used for refinement. TLS refinement cycles (using TLS Motion Determination (*16*)) were combined with validation and model building. Water molecules were located with COOT and refined using ArpWarp from the CCP4 suite. All molecular graphics images were generated using the UCSF Chimera (*17*).

Metal Analysis of Recombinant Glyoxalase II Crystals. Metal analysis was carried out by inductively-coupled plasma (ICP) emission spectroscopy. Purified recombinant protein (50 μg) was dissolved in 1 mL of type I H_2O and analyzed by ICP covering zinc and iron.

Evolutionary Analysis. Phylogenetic relationships were inferred from multiple protein sequence alignment by ClustalW (*18*), slow/accurate algorithm, using the protein weight matrix Gonnet series (available at MegAlign from the DNASTAR Lasergene package, version 7). Protein sequences used in this analysis were *L. infantum* glyoxalase II characterized in this work (GenBank accession no. ABC41261), *Leishmania donovani* glyoxalase II (AAW52503), *Leishmania major* putative glyoxalase II (CAJ02466), *Trypanosoma cruzi* glyoxalase II (AAL96759), *Trypanosoma brucei*, *T. brucei brucei*, glyoxalase II (CAD37800), *Homo sapiens* glyoxalase II (CAA62483), *Arabidopsis thaliana* glyoxalase II (AAF19564), *E. coli* probable (hydroxyacyl)glutathione hydrolase (P0AC84), *Saccharomyces cerevisiae* glyoxalase II (CAA71335), *Canis familiaris* protein similar to (hydroxyacyl)glutathione hydrolase (XP_537013), *Anopheles gambiae* putative member of the metallo-β-lactamase superfamily (XP_310681), *Glossina morsitans* protein fragment (Gmm-6805), *Lutzomyia longipalpis* putative protein containing the conserved domain of the β-lactamase superfamily (NSFM-159f08.p1k), *Aspergillus fumigatus* (hydroxyacyl)-glutathione hydrolase (XP_753369), and *Schizosaccharomyces pombe* predicted (hydroxyacyl)glutathione hydrolase (NP_588246). *G. morsitans* and *Lu. longipalpis* protein sequences were deduced from blast searches (protein vs translated DNA) using the Blast Server available at the Wellcome Trust Sanger Institute Web site (The Pathogen Sequencing Unit).

[1] Abbreviations: *Li*GLO2, *Leishmania infantum* glyoxalase II; T(SH)2, trypanothione.

Table 1: Properties of *L. infantum* Glyoxalase II Gene and Protein

GenBank accession number	
gene	DQ294972
protein	ABC41261
location in the *L. infantum* genome	
chromosome	12
location	bp 98258−99145
length	888 bp
mRNA length[a] (start and stop codons included)	888 bp
no. of amino acids[a]	295
isoelectric point[a] (without a His tag)	6.21
molecular mass[a] (without a His tag)	32.5 kDa
bound metal ion[b]	Zn^{2+} and/or Fe^{2+}
substrate *S*-D-lactoyltrypanothione[b]	
K_m	0.091 mM
specific activity	0.497 U·mg^{-1} of enzyme
k_{cat}	0.28 s^{-1}
k_{cat}/K_m	3.0×10^3 M^{-1}·s^{-1}
activity in *L. infantum* promastigote extracts[c]	0.18 U·mg^{-1} of protein
substrate (*S*-D-lactoylglutathionyl)spermidine[b]	
K_m	0.324 mM
specific activity	6.3 U·mg^{-1} of enzyme
k_{cat}	3.52 s^{-1}
k_{cat}/K_m	1.07×10^4 M^{-1}·s^{-1}

[a] Deduced from the DNA or protein sequence. [b] Experimental data from purified recombinant His-tagged protein. [c] Previously obtained value (*8*).

Enzyme Activity Assay. High-purity methylglyoxal was prepared by acid hydrolysis of methylglyoxal 1,1-dimethyl acetal, followed by fractional distillation under reduced pressure in a nitrogen atmosphere, as described (*8*). Oxidized trypanothione (TS_2; Bachem) and glutathionylspermidine (GspSH; Bachem) were reduced with dithiothreitol, in the proportion of 1 mM thiol to 3.2 mM dithiothreitol, as reported (*8*), immediately prior to reaction. *S*-D-Lactoyltrypanothione (SDL-TSH) and (*S*-D-lactoylglutathionyl)spermidine (SDL-GspSH) were immediately prepared from the corresponding reduced thiol ($T(SH)_2$ or GspSH) and methylglyoxal, using yeast glyoxalase I (2.5 U, Sigma). Methylglyoxal was added in excess (3.34 mM in a 2 mL reaction system), and the hemithioacetal concentration was calculated using the value of 3.0 mM for the dissociation constant (*19*). Glyoxalase I assay was performed at 30 °C in a 2 mL reaction volume, in 0.1 M potassium phosphate buffer, pH 7.0. The assay was performed on an Agilent HP 8453 diode array spectrophotometer, with temperature control and magnetic stirring in the cuvette. The reaction was started by the addition of yeast Glx I. The formation of the thioester was followed at 240 nm, and its concentration was calculated using an ϵ_{240} of 6.5 mM^{-1} cm^{-1} for SDL-TSH and assuming an ϵ_{240} of 3.3 mM^{-1} cm^{-1} for SDL-GspSH (the same values reported for bislactoylglutathione and for monolactoyltrypanothione, respectively (*9*)). Concentrations of SDL-TSH between 0.025 and 0.26 mM, and for SDL-GspSH between 0.05 and 0.48 mM, were prepared. The enzyme was removed after the reaction was completed using Amicon Ultra-4 filters (10 000 NMWL, Millipore Corp.). The recovered solution was used for the *L. infantum* recombinant glyoxalase II (2 μg) activity assay, in the same reaction conditions. The hydrolysis of both thioesters was followed at 240 nm. Activity with *S*-D-lactoylglutathione (Sigma) was also assayed, with two thioester concentrations (0.5 and 1.0 mM). The activity was monitored directly at 240 nm and using the more sensitive DTNB assay (*20*).

Determination of Kinetic Parameters. Single-substrate Michaelis−Menten equation parameters for glyoxalase II (K_m and V) were determined by initial-rate analysis. Nonweighted hyperbolic regression by the method of least-squares was performed with the program Hyper32 (J. S. Easterby, University of Liverpool, U.K., http://www.liv.ac.uk/~jse/software.html).

Activity in Crystals. Crystals were soaked with the substrate *S*-D-lactoyltrypanothione. This was prepared from 5 mM reduced trypanothione and 30 mM methylglyoxal, in a 0.9 mL reaction system, using commercial yeast glyoxalase I (10 U). The enzyme was removed using an Amicon Ultra-4 filter (10 000 NMWL, Millipore Corp.), and the substrate solution was concentrated to 100 mM. The soaking solution contained the substrate (0.5 μL) in 5 μL of 40% PEG 8000, 2 M $MgCl_2$, and 1 M acetate, pH 5.5. An intact crystal was placed in each drop of the soaking solution for 30 min, after which it was frozen in liquid nitrogen.

RESULTS

L. infantum Glyoxalase II Gene and Deduced Protein. Blast searches in the *L. infantum* genome on GeneDB (*21*) revealed only one putative (hydroxyacyl)glutathione hydrolase gene 888 bp in length in chromosome 12 (Table 1). The complete *LiGLO2* gene was amplified from genomic DNA of clone MHOM/MA67ITMAP263, and the sequence was confirmed by sequencing in both directions. The *LiGLO2* sequence (GenBank accession no. DQ294972) shows 99.5% identity to *L. donovani* (GenBank accession no. AY851655), 96.5% identity to *L. major* (GeneDB, LmjF12.0220), and 53.5% identity with human glyoxalase II (GenBank accession no. Q16775).

The deduced protein sequence of 295 amino acid residues clearly identified it as a (hydroxyacyl)glutathione hydrolase belonging to the metallo-β-lactamase superfamily. The predicted molecular mass of 32.5 kDa is comparable to those of other trypanosomatid enzymes (*L. major*, *L. donovani*, and *T. brucei*), but larger than that (29 kDa) of human glyoxalase II.

The isoelectric point (pI) of *L. infantum* glyoxalase II, calculated from the protein sequence, is 6.2 (Table 1), similar

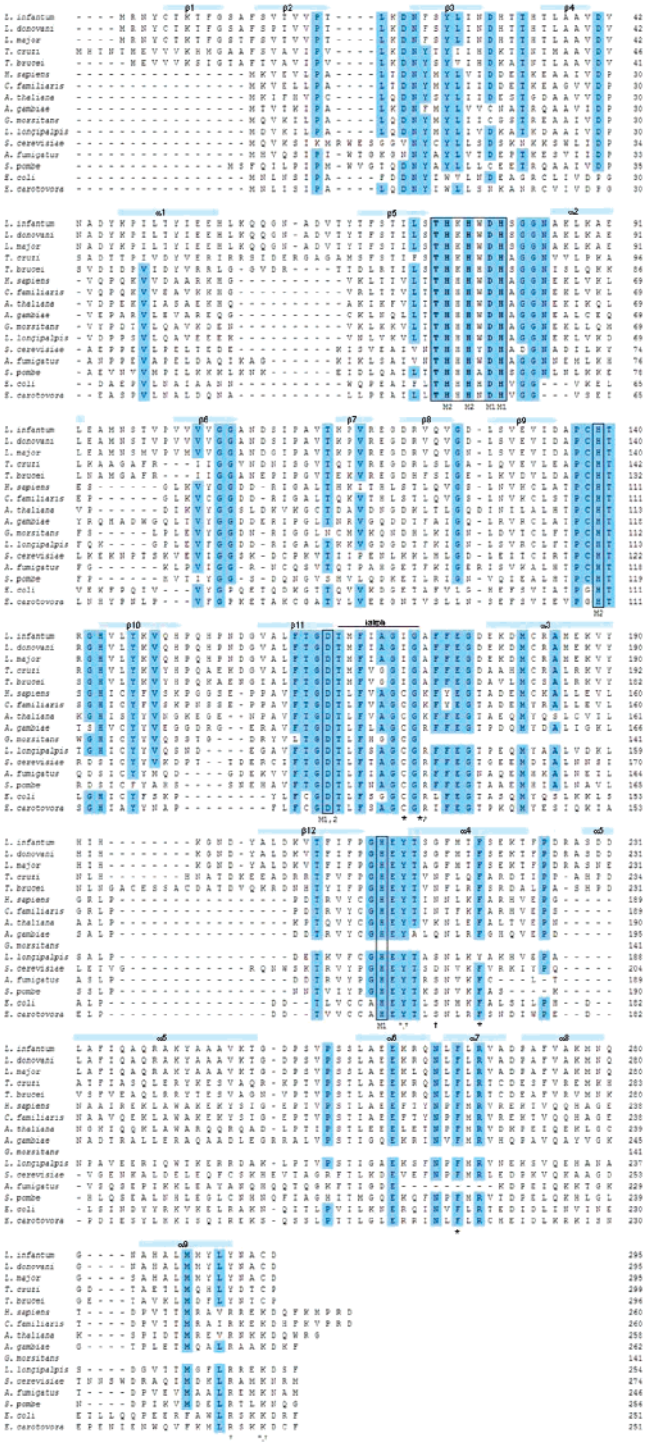

FIGURE 1: Sequence comparison between *L. infantum* glyoxalase II and other glyoxalases II enzymes. The sequences were aligned using ClustalW (*18*), available at MegAlign from the DNASTAR Lasergene package, version 7. *L. infantum* glyoxalase II characterized in this work (GenBank accession no. ABC41261), *L. donovani* glyoxalase II (AAW52503), *L. major* putative glyoxalase II (CAJ02466), *T. cruzi* glyoxalase II (AAL96759), *T. brucei brucei* glyoxalase II (CAD37800), *H. sapiens* glyoxalase II (CAA62483), *A. thaliana* glyoxalase II (AAF19564), *S. cerevisiae* glyoxalase II (CAA71335), *C. familiaris* protein similar to (hydroxyacyl)glutathione hydrolase (XP_537013), *A. gambiae* putative member of the metallo-β-lactamase superfamily (XP_310681), *G. morsitans* protein fragment (Gmm-6805); *Lu. longipalpis* putative protein, containing the conserved β-lactamase superfamily domain (NSFM-159f08.p1k), *A. fumigatus* (hydroxyacyl)glutathione hydrolase (XP_753369), *S. pombe* (hydroxyacyl)glutathione hydrolase predicted (NP_588246), *E. coli* probable (hydroxyacyl)glutathione hydrolase (P0AC84), and *Erwinia carotovora* ssp. *atroseptica* probable (hydroxyacyl)glutathione hydrolase (YP_051431). Residues in gray boxes are conserved in at least 12 of the 16 sequences. Residues of the conserved binding motif TH*X*H*X*DH are in bold and highlighted with a box. Residues responsible for the spermidine fixation in the *L. infantum* sequence are marked with an asterisk. M1, M2, and M1,2 indicate the residues in *L. infantum* that bind metal (zinc or iron) 1, metal 2, or both, respectively. Residues marked with a dagger are responsible for the glutathione binding in glyoxalase II from *H. sapiens*. The indicated secondary structure is from *L. infantum* glyoxalase II.

to 6.0−6.5 from *T. brucei* (*9*), 6.0 for *L. donovani* (*22*), and 6.2 for *A. thaliana* (*23*). The obtained value differs from the 8.5 pI for the human glyoxalase II, determined by isoelectric focusing (*24*).

Table 2: Crystallographic Data Collection and Refinement Statistics of Native Glyoxalase II and with the Product D-Lactate

	*Li*GLO2−spermidine	*Li*GLO2−D-lactate
space group	$C222_1$	$C222_1$
unit cell parameters (Å)	$a = 66.7$, $b = 89.0$, $c = 85.9$	$a = 67.2$, $b = 89.1$, $c = 86.0$
source	ID23-1	ID23-1
wavelength (Å)	0.954	0.954
no. of unique reflns	23 962	20 692
resolution limits (Å)	53.4−1.8	53.6−1.9
redundancy	5.7 (5.8)	13.8 (14.1)
R_{merge}[a] (%)	6.9 (46.8)	8.7 (48.8)
completeness (%)	99.8 (100)	100 (100)
$\langle I/\sigma(I)\rangle$	6.5 (1.6)	5.1 (1.5)

[a] $R_{merge} = \sum_h\sum_l|I_{hl} - \langle I_h\rangle|/\sum_h\sum_l\langle I_h\rangle$, where I_l is the lth observation of reflection h and $\langle I_h\rangle$ is the weighted average intensity for all observations l of reflection h.

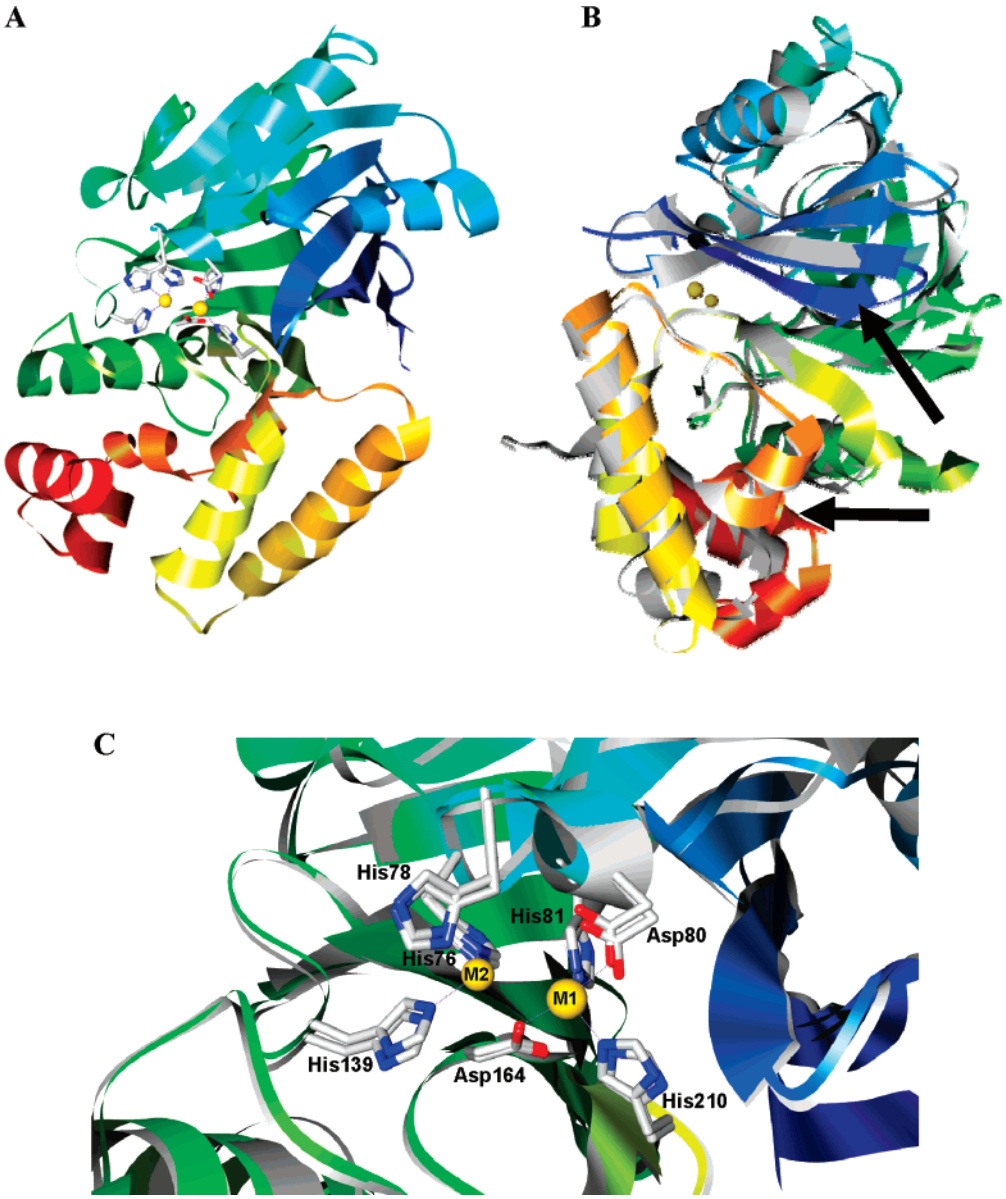

FIGURE 2: Comparison of the overall structure and active site of *L. infantum* and human glyoxalase II. *L. infantum* (A, rainbow color) and human glyoxalase II (gray) superimpose (B) with a root-mean-square deviation of 1.60 Å (using 191 Cα atoms); arrows point to the β sheet and α helix present in *Li*GLO2−spermidine and not in the human glyoxalase II. (C) Details of the superposition of the active site of the two structures showing the high homology of the active site. Metals (M1 and M2) are coordinated by the same residues; identified residues are from *L. infantum*. The figure was prepared using UCSF Chimera (*17*).

The *L. infantum* deduced protein contains the highly conserved metal binding motif TH*X*H*X*DH, common to all glyoxalases II (Figure 1), including human, yeast, and *Arabidopsis*, and also present in the metallo-β-lactamase family, which are known to require Zn(II) (*23*, *25*, *26*).

Overexpression and Purification of Recombinant Glyoxalase II. The *L. infantum LiGLO2* gene was cloned into the pET-28a expression vector and this construct transformed into *E. coli* BL21-codon plus cells. Small-scale growth cultures were used to optimize overexpression conditions for

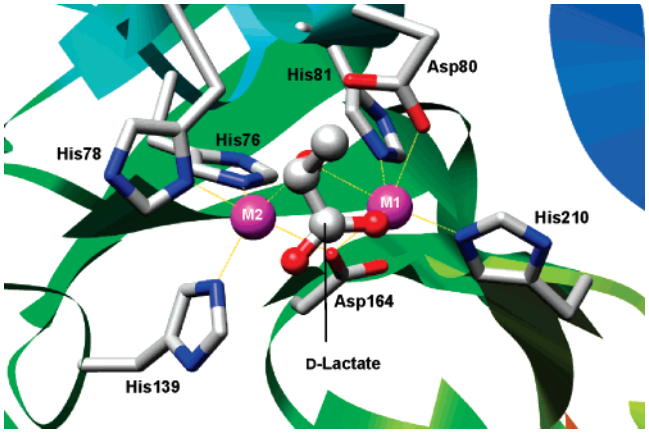

FIGURE 3: Details of the structure of *L. infantum* with D-lactate (*Li*GLO2−D-lactate) located at the active site. Residues from the active site interacting with the metals (M1 and M2) and with the D-lactate molecule are shown. The figure was prepared in UCSF Chimera (*17*).

His-tagged glyoxalase II. Purification was performed by metal affinity chromatography and yielded 25 mg of pure protein from 3 L of culture. The purity of the recombinant His-*Li*GLO2 was ≥95%, as estimated by SDS−PAGE and gel-filtration chromatography (data not shown), and the apparent molecular mass of 32 kDa was in accordance with the 32.5 kDa deduced from the protein sequence.

Final Structures. The *L. infantum* glyoxalase II structure with spermidine (*Li*GLO2−spermidine) was refined against data extending to a d_{min} of 1.8 Å in space group $C222_1$, to an *R* factor of 17.2%, and to a corresponding R_{free} (*27*) of 19.6%. The final enzyme structure has 287 residues, and the Matthews coefficient is 1.95 $Å^3Da^{-1}$, corresponding to a solvent content of ∼37%, assuming the presence of a single molecule in the asymmetric unit (PDB entry 2P18). Data collection and processing statistics are given in Table 2.

Associated with each protein molecule there are two metal ions, an acetate molecule and a spermidine molecule. A total of 188 water molecules were found in the structure. The average temperature factor of the protein is 23.9 $Å^2$. For the final structure, the rmsd's from ideal bond lengths and bond angles were 0.015 Å and 1.519°, respectively, and no outlier residues were found in the Ramachandran plot.

L. infantum glyoxalase II is a 295 amino acid metalloprotein. Like the previously described human glyoxalase II structure (*10*), the *L. infantum* glyoxalase II monomer is arranged in two domains. The N-terminal domain, including residues 1−209, has a topology of a four-layered β sandwich with two mixed β sheets of four and seven β strands flanked by two long α helices. The first half of the sandwich folds as a $\beta\beta\beta\beta\alpha\beta\alpha\beta\beta$ motif and the second half as a $\beta\beta\beta\beta\alpha\beta$ motif. Thus, the unit $\beta\beta\beta\beta\alpha\beta$ is common to the two halves ($\beta_1\beta_2\beta_3\beta_4\alpha_1\beta_5$ and $\beta_8\beta_9\beta_{10}\beta_{11}\alpha_3\beta_{12}$). The C-terminal domain, including residues 210−295, is an all α helical domain located at the edge of the N-terminal domain. Preceding the helix α_6, a section of chain extends the second sheet of the N-terminal domain by hydrogen bonding to β_{11}. A β hairpin loop of the N-terminal domain, situated after β_{11}, protrudes into the C-terminal domain, making hydrogen-bonding and hydrophobic interactions with residues on helices α_4 and α_6 (Figure 2).

The *L. infantum* glyoxalase II structure is similar to the whole structure of the human homologue (PDB 1QH3), these

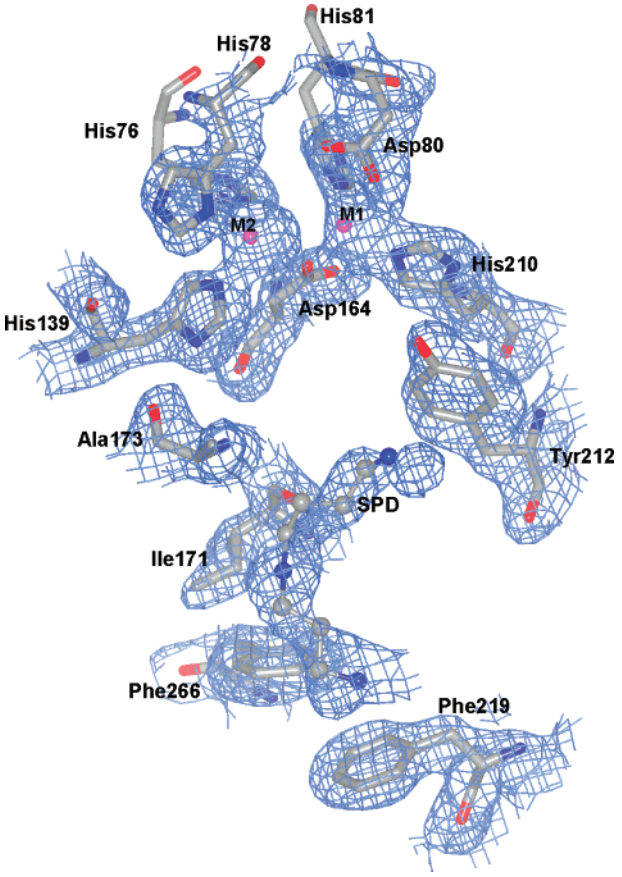

FIGURE 4: *L. infantum* glyoxalase II substrate binding site (*Li*GLO2−spermidine). Details of the active site showing the residues interacting with the metals (M1 and M2) and the spermidine molecule (SPD), with overlaid electron density contoured at 1 σ (omit map computed without both metals and the spermidine molecule). The figure was prepared in CCP4mg (*30*, *31*).

structures being superimposed with an rmsd of 1.60 Å (using 191 Cα atoms). Compared to the human glyoxalase II, *L. infantum* glyoxalase II has one extra β strand at the N-terminal and an extra α helix at the C-terminal domain. As a consequence, the referred $\beta\beta\beta\beta\alpha\beta$ motif, common to the two halves of the sandwich, is slightly longer than the human homologue, but identical to that on other metallo-β-lactamases (*28*).

A crystal structure containing D-lactate in the active site (*Li*GLO2−D-lactate), one of the reaction products, was obtained after soaking for 30 min with the substrate (Figure 4). Hence, the protein remained active in the crystal form. As the previous crystals, this crystal belonged to the space group $C222_1$, with unit cell parameters approximately identical to those reported previously: $a = 67.2$ Å, $b = 89.1$ Å, $c = 86.0$ Å. The Matthews coefficient was 1.97 $Å^3$ Da^{-1}, corresponding to a solvent content of ∼38%, assuming the presence of a single molecule in the asymmetric unit (PDB 2P1E). The *L. infantum* glyoxalase II structure containing D-lactate was refined against data extending to a d_{min} of 1.9 Å, to an *R* factor of 18.3%, and to a corresponding R_{free} of 22.0%. The final structure containing D-lactate is very similar to the native *L. infantum* glyoxalase II model and has an average temperature factor of 26.2 $Å^2$. The average temperature factor of the D-lactate molecule was 30.1 $Å^2$, and this molecule was located between the two metal ions, separated by 3.58 Å. It was bound to both metals through its O3 atom,

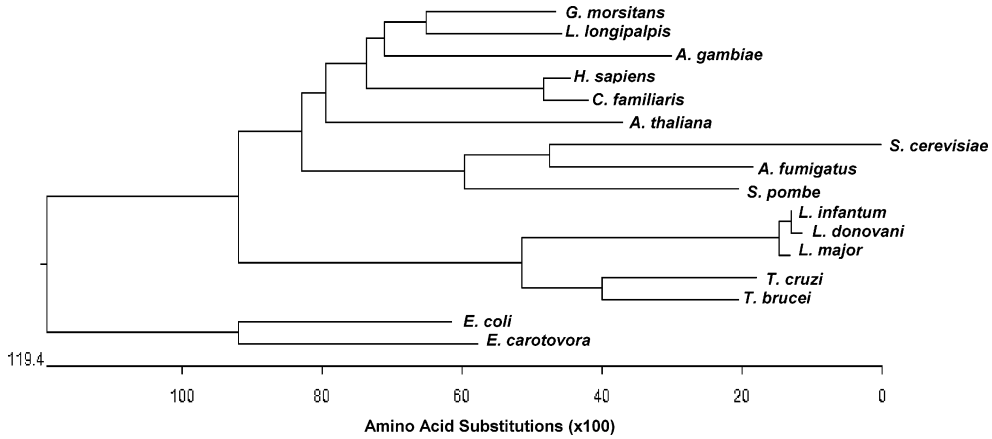

FIGURE 5: Phylogenetic tree of alignment from Figure 1, between *L. infantum* glyoxalase II and other glyoxalase II or putative (hydroxyacyl)-glutathione hydrolase enzymes. Rectangular phylogram, performed from the alignment using MegAlign from DNASTAR Lasergene (branches are proportional to the genetic distance). Species are the same as indicated in Figure 1.

at distances of 2.30 and 2.68 Å from metals 1 and 2, respectively. The bridge established by this latter atom replaces the water molecule present in the *Li*GLO2−spermidine structure. The D-lactate was also bound to metal 1 through its O1 and O2 atoms, at distances of 2.87 and 2.14 Å, respectively, which replaces the bridge established by the acetate molecule oxygen atoms in the *Li*GLO2−spermidine structure. This is the only major change caused by the insertion of D-lactate into the structure. There are a total of 102 water molecules in this structure. For the final structure, the rmsd's from ideal bond lengths and bond angles were 0.016 Å and 1.540°, respectively, and no outlier residues were found in a stringent boundary Ramachandran plot.

Active Site. Previous sequence analysis revealed the presence of the highly conserved metal binding motif TH*X*H*X*DH in trypanosomatid and all other glyoxalase II proteins (Figure 1). The active site extends across the domain interface and harbors a metal binding site. There was clear electron density for a binuclear metal binding site in the domain interface. The average temperature factor of each zinc atom was 17 and 18 Å^2, whereas for each iron atom it was 15 Å^2. Metal analysis (ICP) revealed that the enzyme binds 1.54 mol of zinc/mol of protein and 0.05 mol of iron/mol of protein, suggesting that zinc is the main metal present in the active site, in accordance with the results obtained by measuring the temperature factor. Both pieces of data indicate that this enzyme is able to bind either zinc or iron. In *T. brucei* glyoxalase II, sequence analysis pointed to zinc as the main metal (*9*), whereas in glyoxalase II from *A. thaliana*, a 1:2 zinc:iron ratio of the binuclear center, essential for substrate binding and catalysis, was reported (*25*). Although the human glyoxalase II structure revealed the presence of two zinc ions, it was also not possible to discriminate between zinc and iron (*10*).

The two metals from the *L. infantum* glyoxalase II structure, separated by 3.32 Å, are coordinated by seven amino acid residues from three different regions of the N-terminal domain and bridged by an acetate molecule, a water molecule, and the Asp164. This latter residue seems to be in a more favorable position for metal 1 coordination than for metal 2, as the Asp164 oxygen atom is further away from metal 2 (2.51 Å) than from metal 1 (2.09 Å). Metal 1 interacts with Asp80 (2.26 Å), His81 (2.10 Å), Asp164 (2.09 Å), and His210 (2.08 Å), whereas metal 2 is coordinated by His76 (2.27 Å), His78 (2.13 Å), His139 (2.06 Å), and Asp164 (2.51 Å) (Figure 3). This characteristic tetrahedral coordination to each metal is identical to that reported to the human glyoxalase II structure when bound to a glutathione analogue (*10*).

Substrate Binding Site. The thiol replacement in the glyoxalase system of trypanosomatids suggests that these enzymes are different from all other eukaryotic glyoxalases. Indeed, the human glyoxalase II structure revealed three conserved basic residues involved in thioester binding, Arg249, Lys143, and Lys252 (*10*), also present in almost all eukaryotic glyoxalases II. These residues are found neither in *L. infantum* protein nor in the proteins from *T. brucei* or other kinetoplastid organisms (*9*). *L. infantum* glyoxalase II does not use lactoylglutathione as a substrate, as confirmed by direct assay at 240 nm and by the more sensitive DTNB assay. A spermidine molecule was bound to the recombinant *L. infantum* enzyme and crystallized close to the active site. This molecule has an average temperature factor of 25.8 Å^2 and interacts with Ile171, Ala173, Tyr212, Phe219, and Phe266 (Figure 3). Curiously, the Phe266 residue, interacting with the spermidine, is present in the extra α helix at the C-terminal domain from the *L. infantum* glyoxalase II. Although it also exists in the human glyoxalase II (Phe224), this residue does not seem to interact with the substrate in this enzyme.

Glyoxalase II Kinetics: Specificity for Thioesters of Spermidine−Glutathione Conjugates. In cell-free extracts, *L. infantum* glyoxalase II is highly specific for *S*-D-lactoyltrypanothione and does not show activity with *S*-D-lactoylglutathione (*8*). Structural data revealed a spermidine molecule accommodated in the substrate binding site. It might be possible that the glutathionylspermidine-derived thioester is also a substrate. Recombinant *Li*GLO2 was assayed for both trypanothione- and glutathionylspermidine-derived thioesters. With bislactoyltrypanothione as a substrate, a K_m of 0.091 mM and a K_{cat} of 0.28 s^{-1} were determined (Table 1). When the substrate is the glutathionylspermidine-derived thioester, a K_m of 0.32 mM and a K_{cat} of 3.52 s^{-1} were obtained (Table 1). K_m values are in good agreement with those reported in cell-free extracts (*8*). As expected, no activity was detected with *S*-D-lactoylglutathione. Results confirmed that the *Li*GLO2 shows specific affinity toward

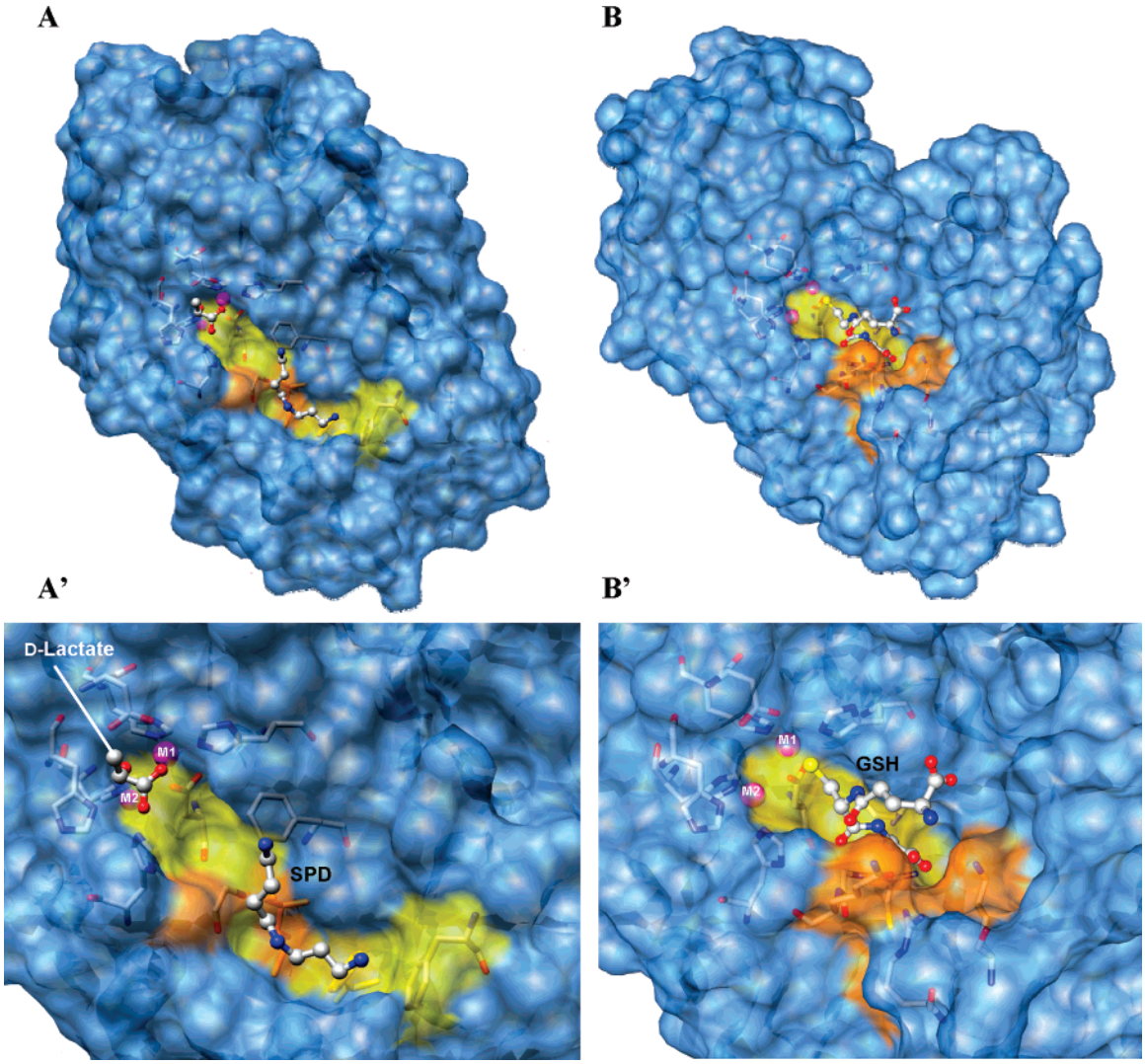

FIGURE 6: Molecular surfaces of *L. infantum* and human glyoxalase II proteins. (A) Superposition of *Li*GLO2−spermidine (PDB 2P18) with the *Li*GLO2−D-lactate structure (PDB 2P1E). (A′) Details of the active and substrate binding sites, showing the spermidine and D-lactate molecules in the pocket that could easily harbor the lactoyltrypanothione. Metals M1 and M2 are indicated. Residues in the pocket are colored in yellow and orange. Orange-colored residues, Ile171 and Ala173, are absent from the human enzyme. (B) Human glyoxalase II containing a glutathione molecule (GSH) at the substrate binding site (PDB 1QH5, chain A). (B′) Details of the active and substrate binding sites. Metals M1 and M2 are indicated. The cavity harboring the glutathione (in yellow and orange) is clearly different from that of *Li*GLO2. Orange-colored residues, Lys143, Arg249, and Lys252, are absent from trypanosomatid enzymes. The figure was prepared in UCSF Chimera (*17*).

spermidine−glutathione conjugate-derived thioesters. Although kinetics point to the glutathionylspermidine-derived thioester as the preferred substrate, glutathionylspermidine exists in *L. infantum* in much lower concentration than trypanothione (unpublished results), lactoyltrypanothione being the most probable physiological substrate for *Li*GLO2.

Trypanothione Specificity: Structural and Evolutionary Analysis. Kinetoplastida are protozoan organisms that diverged early in evolution from other eukaryotes (*2*). One particular characteristic shared by these parasites is the functional replacement of glutathione by a glutathione−spermidine thiol conjugate, trypanothione (*3*). Consequently, their enzymes depend on trypanothione and replace the glutathione-dependent ones from all other eukaryotic organisms and prokaryotes. Examples are the enzymes of the glyoxalase pathway, which preferably use trypanothione as a cofactor, glyoxalase II being exclusively dependent on the trypanothione thioester (*7*−*9*, *29*). Trypanosomatid glyoxalases II follow kinetoplastida evolution, diverting early from other eukaryotic organisms into a separate group (Figure 5). The other branch for eukaryotes is divided into two other major groups, one including fungi and the second containing other eukaryotes, including trypanosomatid's hosts (human and dog) and vectors *G. morsitans* (tsetse fly), *Lu. longipalpis* (the phlebotomine sand fly responsible for the transmission of *Leishmania* in the New World), and *A. gambiae* (malaria mosquito) proteins (Figure 5). The prokaryotic glyoxalases II analyzed, *E. coli* and *Er. carotovora*, are clearly separated from eukaryotic proteins, and the highest divergence obtained between them and trypanosomatid proteins clearly eliminates a prokaryotic origin for the parasite's enzymes (between 167% and 170% divergence, with only 29% identity; the percent identity compares sequences directly, without accounting for phylogenetic relationships, and divergence is calculated by comparing sequence pairs in relation to the reconstructed phylogeny).

On the basis of the three-dimensional structures of *L. infantum* (this work) and human glyoxalases II (*10*), and

taking into account the protein sequence alignment between other homologous proteins, amino acid substitutions in the various sequences were analyzed in a structural and functional context. In all species, the residues involved in metal binding are absolutely conserved (Figure 1, residues marked M1, M2, and M1,2). These residues are common to all species and correspond exactly to the same metal, metal 1, metal 2, or both, in human glyoxalase II (*10*). Concerning substrate binding, residue conservation is not observed between trypanosomatid and other eukaryotic glyoxalase II enzymes. This is an expectable result, since trypanosomatids use a trypanothione-derived thioester as the substrate, whereas all other eukaryotic glyoxalases II hydrolyze lactoylglutathione. Comparing both enzymes (Figure 6), differences at the substrate binding sites are clearly observed. Trypanosomatids lack the Lys143, Arg249, and Lys252 (Figure 6B′, in orange) responsible for glutathione binding in human glyoxalase II (*10*). On the other hand, *L. infantum* glyoxalase II has Ile171 (absent from the human enzyme, Figure 6A′, in orange) and both Phe219 and Phe266 strategically positioned to bind the spermidine moiety of the thioester (Figure 6A′). These two phenylalanine residues, although present in the human GLO2 at positions 182 and 224, respectively, are absent from the substrate binding site. In *L. infantum*, superposition of both structures containing the spermidine and the molecule of D-lactate located between the two metal ions allows us to speculate on the possible position of the glutathione moiety of trypanothione (Figure 6A,A′), being clear how the trypanosomatid enzyme evolved to accommodate the thioester spermidine moiety.

DISCUSSION

The crystal structure of glyoxalase II from *L. infantum* presented here is the first structure from a trypanosomatid. Previously, only the human (PDB 1QH5), *Arabidopsis* (PDB 1XM8 and PDB 2Q42), and *Salmonella thyphimurium* (PDB 2OBW) structures were determined. The most remarkable feature is the electron density found close to the active center that is consistent with a spermidine molecule. This means that the recombinant glyoxalase II was able to bind a molecule that is part of the physiological substrate. Since the enzyme is absolutely specific for lactoyltrypanothione substrates and shows no activity with lactoylglutathione, it was possible to elucidate the molecular mechanism of trypanothione specificity for glyoxalase II. This discovery has far-reaching consequences regarding the design of specific inhibitors for trypanothione-dependent enzymes. Given its uniqueness and importance in trypanosomatids, these enzymes are by far the most promising therapeutic targets. The sequence and structure of glyoxalase II from *L. infantum* also provide hints regarding the evolution of trypanosomatids. They diverged early from other eukaryotes and are not related at all to prokaryotic enzymes.

ACKNOWLEDGMENT

We thank the ESRF in Grenoble, France, for the data collection support. We also acknowledge Dr. Maria João Romão for providing crystallographic data from the Laboratório de Cristalografia de Raios-X at the Faculdade de Ciências e Tecnologia, Universidade Nova de Lisboa, Portugal.

REFERENCES

1. Michels, P. A., Hannaert, V., and Bringaud, F. (2000) Metabolic aspects of glycosomes in trypanosomatidae—new data and views, *Parasitol. Today 16*, 482−489.
2. Hannaert, V., Bringaud, F., Opperdoes, F. R., and Michels, P. A. (2003) Evolution of energy metabolism and its compartmentation in kinetoplastida, *Kinetoplastid Biol. Dis. 2*, 11.
3. Muller, S., Liebau, E., Walter, R. D., and Krauth-Siegel, R. L. (2003) Thiol-based redox metabolism of protozoan parasites, *Trends Parasitol. 19*, 320−328.
4. Flohe, L., Hecht, H. J., and Steinert, P. (1999) Glutathione and trypanothione in parasitic hydroperoxide metabolism, *Free Radicals Biol. Med. 27*, 966−984.
5. Krauth-Siegel, R. L., Bauer, H., and Schirmer, R. H. (2005) Dithiol proteins as guardians of the intracellular redox milieu in parasites: old and new drug targets in trypanosomes and malaria-causing plasmodia, *Angew. Chem., Int. Ed. 44*, 690−715.
6. Thornalley, P. J. (1990) The glyoxalase system: new developments towards functional characterization of a metabolic pathway fundamental to biological life, *Biochem. J. 269*, 1−11.
7. Vickers, T. J., Greig, N., and Fairlamb, A. H. (2004) A trypanothione-dependent glyoxalase I with a prokaryotic ancestry in *Leishmania major*, *Proc. Natl. Acad. Sci. U.S.A. 101*, 13186−13191.
8. Sousa Silva, M., Ferreira, A. E., Tomas, A. M., Cordeiro, C., and Ponces Freire, A. (2005) Quantitative assessment of the glyoxalase pathway in *Leishmania infantum* as a therapeutic target by modelling and computer simulation, *FEBS J. 272*, 2388−2398.
9. Irsch, T., and Krauth-Siegel, R. L. (2004) Glyoxalase II of African trypanosomes is trypanothione-dependent, *J. Biol. Chem. 279*, 22209−22217.
10. Cameron, A. D., Ridderstrom, M., Olin, B., and Mannervik, B. (1999) Crystal structure of human glyoxalase II and its complex with a glutathione thiolester substrate analogue, *Structure Folding Des. 7*, 1067−1078.
11. Trincao, J., Sousa, Silva, M., Barata, L., Bonifacio, C., Carvalho, S., Tomas, A. M., Ferreira, A. E. N., Cordeiro, C., Ponces, Freire, A., and Romao, M. J. (2006) Purification, crystallization and preliminary X-ray diffraction analysis of the glyoxalase II from Leishmania infantum, *Acta Crystallogr., Sect. F: Struct. Biol. Cryst. Commun. 62*, 805−807.
12. Leslie, A. G. W. (1992) Recent changes to the MOSFLM package for processing film and image plate data, *Joint CCP4 and ESF-EACBM Newsletters on Protein Crystallography*, Vol. 26, Daresbury Laboratory, Warrington, U.K.
13. (1994) The CCP4 suite: programs for protein crystallography, *Acta Crystallogr., Sect. D: Biol. Crystallogr. 50*, 760−763.
14. Read, R. J. (2001) Pushing the boundaries of molecular replacement with maximum likelihood, *Acta Crystallogr., Sect. D: Biol. Crystallogr. 57*, 1373−1382.
15. Emsley, P., and Cowtan, K. (2004) Coot: model-building tools for molecular graphics, *Acta Crystallogr., Sect. D: Biol. Crystallogr. 60*, 2126−2132.
16. Painter, J., and Merritt, E. A. (2006) Optimal description of a protein structure in terms of multiple groups undergoing TLS motion, *Acta Crystallogr., Sect. D: Biol. Crystallogr. 62*, 439−450.
17. Pettersen, E. F., Goddard, T. D., Huang, C. C., Couch, G. S., Greenblatt, D. M., Meng, E. C., and Ferrin, T. E. (2004) UCSF Chimera−a visualization system for exploratory research and analysis, *J. Comput. Chem. 25*, 1605−1612.
18. Thompson, J. D., Higgins, D. G., and Gibson, T. J. (1994) CLUSTAL W: improving the sensitivity of progressive multiple sequence alignment through sequence weighting, position-specific gap penalties and weight matrix choice, *Nucleic Acids Res. 22*, 4673−4680.
19. Vander, Jagt, D. L., Han, L. P., and Lehman, C. H. (1972) Kinetic evaluation of substrate specificity in the glyoxalase-I-catalyzed disproportionation of ketoaldehydes, *Biochemistry 11*, 3735−3740.
20. Martins, A. M., Cordeiro, C., and Freire, A. P. (1999) Glyoxalase II in *Saccharomyces cerevisiae*: *In situ* kinetics using the 5,5′-dithiobis(2-nitrobenzoic acid) assay, *Arch. Biochem. Biophys. 366*, 15−20.
21. Hertz-Fowler, C., Peacock, C. S., Wood, V., Aslett, M., Kerhornou, A., Mooney, P., Tivey, A., Berriman, M., Hall, N., Rutherford, K., Parkhill, J., Ivens, A. C., Rajandream, M. A., and Barrell, B.

(2004) GeneDB: a resource for prokaryotic and eukaryotic organisms, *Nucleic Acids Res. 32*, D339−D343.
22. Padmanabhan, P. K., Mukherjee, A., Singh, S., Chattopadhyaya, S., Gowri, V. S., Myler, P. J., Srinivasan, N., and Madhubala, R. (2005) Glyoxalase I from Leishmania donovani: a potential target for anti-parasite drug, *Biochem. Biophys. Res. Commun. 337*, 1237−1248.
23. Crowder, M. W., Maiti, M. K., Banovic, L., and Makaroff, C. A. (1997) Glyoxalase II from *A. thaliana* requires Zn(II) for catalytic activity, *FEBS Lett. 418*, 351−354.
24. Ridderstrom, M., Saccucci, F., Hellman, U., Bergman, T., Principato, G., and Mannervik, B. (1996) Molecular cloning, heterologous expression, and characterization of human glyoxalase II, *J. Biol. Chem. 271*, 319−323.
25. Zang, T. M., Hollman, D. A., Crawford, P. A., Crowder, M. W., and Makaroff, C. A. (2001) Arabidopsis glyoxalase II contains a zinc/iron binuclear metal center that is essential for substrate binding and catalysis, *J. Biol. Chem. 276*, 4788−4795.
26. Concha, N. O., Rasmussen, B. A., Bush, K., and Herzberg, O. (1996) Crystal structure of the wide-spectrum binuclear zinc beta-lactamase from Bacteroides fragilis, *Structure 4*, 823−836.
27. Brunger, A. T. (1992) Free R-Value - a Novel Statistical Quantity for Assessing the Accuracy of Crystal-Structures, *Nature 355*, 472−475.
28. Carfi, A., Pares, S., Duee, E., Galleni, M., Duez, C., Frere, J. M., and Dideberg, O. (1995) The 3-D structure of a zinc metallo-beta-lactamase from Bacillus cereus reveals a new type of protein fold, *EMBO J. 14*, 4914−4921.
29. Ariza, A., Vickers, T. J., Greig, N., Armour, K. A., Dixon, M. J., Eggleston, I. M., Fairlamb, A. H., and Bond, C. S. (2006) Specificity of the trypanothione-dependent Leishmania major glyoxalase I: structure and biochemical comparison with the human enzyme, *Mol. Microbiol. 59*, 1239−1248.
30. Potterton, E., McNicholas, S., Krissinel, E., Cowtan, K., and Noble, M. (2002) The CCP4 molecular-graphics project, *Acta Crystallogr., Sect. D: Biol. Crystallogr. 58*, 1955−1957.
31. Potterton, L., McNicholas, S., Krissinel, E., Gruber, J., Cowtan, K., Emsley, P., Murshudov, G. N., Cohen, S., Perrakis, A., and Noble, M. (2004) Developments in the CCP4 molecular-graphics project, *Acta Crystallogr., Sect. D: Biol. Crystallogr. 60*, 2288−2294.

BI700989M